Journal of Cleaner Production 294 (2021) 126342

Contents lists available at ScienceDirect

Journal of Cleaner Production

journal homepage: www.elsevier.com/locate/jclepro

Microbial community assembly and metabolic function in top layers of slow sand filters for drinking water production

Lihua Chen [a, b, 1], Yujia Zhai [b, c, d, 1], Ed van der Mark [e], Gang Liu [a, b, *], Walter van der Meer [c, d], Gertjan Medema [b, f, g]

[a] Key Laboratory of Drinking Water Science and Technology, Research Centre for Eco-Environmental Sciences, Chinese Academy of Sciences, Beijing, 100085, PR China
[b] Sanitary Engineering, Department of Water Management, Faculty of Civil Engineering and Geosciences, Delft University of Technology, P.O. Box 5048, 2600, GA Delft, the Netherlands
[c] Science and Technology, University of Twente, P.O. Box 217, 7500, AE, Enschede, the Netherlands
[d] Oasen Water Company, PO BOX 122, 2800, AC, Gouda, the Netherlands
[e] Dunea Water Company, PO BOX 756, 2700, AT, Zoetermeer, the Netherlands
[f] KWR Water Research Institute, P.O. Box 1072, 3430, BB, Nieuwegein, the Netherlands
[g] Michigan State University, 1405 S Harrison Rd East-Lansing, 48823, USA

ARTICLE INFO

Article history:
Received 4 October 2020
Received in revised form
8 January 2021
Accepted 8 February 2021
Available online 10 February 2021

Keywords:
Slow sand filters
Top layers
Schmutzdecke
Microbial community assembly
Predicted metabolic function
Neutral community model

ABSTRACT

Slow sand filters (SSFs) are widely applied to treat potable water; the removal of contaminants (e.g., particles, organic matter, and microorganism) occurs primarily in the top layer. However, the development of the microbial community and its metabolic function is still poorly understood. In the present study, we analyzed the microbial quantity and community of the influents sampled from the effluent of the last step (rapid sand filtration) and of the top layers of SSFs (Schmutzdecke, 0–2 cm, 4–6 cm, 8–10 cm) sampled near terminal head loss when the Schmutzdecke (SCM) was most developed in two full-scale drinking water treatment plants (DWTPs). The two DWTPs use the same artificially recharged groundwater source. The biomass in the filter, quantified by flow cytometric intact cell counts (ICC) and adenosine triphosphate (ATP), decreased rapidly along the depth till 8–10 cm (>1 log TCC; >75% ATP); the decrease was most pronounced from the SCM to the surface sand layer (0–2 cm), after which the biomass stabilized quickly at lower depths (2–10 cm). Remarkably, beta diversity showed that SSFs layers of the same depth in two DWTPs with distinctive filter age and plant location clustered together, which indicated their insignificant effects in shaping microbial communities in SSFs. The alpha diversity indices followed the trend of the biomass, suggesting more active and diverse communities in SCM layer. PICRUSt-based function prediction revealed significant over-representation of metabolism and degradation of complex organic matters (e.g., butanoate, propanoate, xenobiotic, D-Alanine, chloroalkene, and bisphenol) in SCM layer, the functional importance of which was confirmed by the co-occurrence patterns of the dominant taxa and metabolic functions. Using an island biogeography model, we found that microbial communities in SSFs were strongly assembled by selection (68 OTUs, 50.0% sequences), rather than by simple accumulation of the microbial communities in the influents (120 OTUs, 44.8% sequences). Our findings enhance the understanding of microbial community assembly and of metabolic function in the top layers of SSFs, and constitute a valuable contribution to optimizing the design and operation of biofilters in full-scale DWTPs.

1. Introduction

Slow sand filters (SSFs) have been widely used in drinking water treatment to produce biological stable drinking water, which have been recognized for their low energy and chemical consumption, high efficiency, and simple operation (Haig et al., 2011). As the

* Corresponding author. Key Laboratory of Drinking Water Science and Technology, Research Centre for Eco-Environmental Sciences, Chinese Academy of Sciences, Beijing, 100085, PR China.
E-mail addresses: gliu@rcees.ac.cn, g.liu-1@tudelft.nl (G. Liu).
[1] The two authors contribute equally.

https://doi.org/10.1016/j.jclepro.2021.126342

water flows through, particles, organic matter, and microbes present in the source water are removed by physicochemical and microbiological processes in the sand bed (Haig et al., 2011, 2014). Previous studies have demonstrated that the high purification efficiency of SSFs was principally related to the biodegradation of organic contaminants (Haig et al., 2016; Prenafeta-Boldu et al., 2017; Oh et al., 2018), which has been attributed mostly to the Schmutzdecke (SCM) layer (surface and top 1–1.5 cm) in the sand filters (Campos et al., 2002; Nitzsche et al., 2015). However, the lack of a fundamental understanding of the biological processes in SSFs has held back the further optimization and promotion of the technology.

Efforts have been made to increase understanding of the microbial ecology and biological processes in SSFs. For example, previous studies have found that the diversity and function of microbial communities in such engineered systems are closely related to treatment performances (Oh et al., 2018; Zhang et al., 2018; Haig et al., 2015). Moreover, a number of studies have attempted to link the purification mechanisms and the associated responsible populations (Wang et al., 2010; Martineau et al., 2015; Li et al., 2013). However, such studies focused mainly on specific purification mechanisms, like nitrogen removal by nitrification and denitrification (Aslan and Cakici, 2007), and Mn-oxidization by certain bacteria (i.e., *Leptothix*, *Gallionella*, *Siderocapsa*, *Crenothix*, *Hyphomicrobium*, and *Metalloaenium*) (Nitzsche et al., 2015; Li et al., 2013; Abu Hasan et al., 2012). Most of the available research was performed on lab-scale microcosms (Manav Demir et al., 2018; Seeger et al., 2016; Grace et al., 2016), which were established under certain controlled parameters, but not in field. To date, studies addressing the microbial communities and their metabolic capacities in SSFs are still limited, which is attributed to the limitations on the application of advanced molecular technologies to conventional biological processes in the field and on the accessibility of full-scale filters. Oh et al. (2018) reported a metagenomic characterization of biofilters in a full-scale drinking water treatment plant, which included a rapid sand filter, a granular activated carbon filter, and a SSF, and provided valuable insights into the microbial community phylogenetic structure, colonization pattern, and metabolic capacity (Oh et al., 2018). However, only the SCM from each type of biofilter in a single plant was sampled and analyzed. Studies of the vertical distribution of the top layers, and multiple-plant studies, which are important for understanding the development of microbial communities in SSFs, are still lacking.

Beyond scanning the microbial communities to determine "who is present" and "how the composition changes spatially or temporally", it is critical that we understand the rules governing community assembly in SSFs. Previous studies focused mainly on how deterministic factors (i.e., taxa competition and niche differentiation) affect the target communities (Nair et al., 2014; Pompei et al., 2017). Using a neutral community model and a column simulation system, Vignola et al. (2018) found both niche and neutral factors acted on microbial community assembly in sand filters (Vignola et al., 2018). Multi-layer sampling from full-scale operational sand filters is still needed to study the development and assembly of microbial communities in SSFs and its metabolic functions.

The present study targets the SCM-10 cm top layers of SSFs in two full-scale DWTPs that use the same artificial recharged groundwater as a source. The objective is to investigate the vertical distribution of the quantity and communities of microbes in the top layers, and to explore the assembly of the microbial communities and their metabolic functions. The biomass was quantified by ATP and intact cell counts (ICC), and 16S rRNA sequencing (Illumina MiSeq) combined with a modified neutral community model (NCM) was performed to investigate the microbial community assembly. Phylogenetic Investigation of Communities by Reconstruction of Unobserved States (PICRUSt) based on 16S rRNA sequencing data was used to predict the metabolic functions.

2. Material and methods

2.1. Description of SSFs

The study was performed on two full-scale SSFs at Dunea DWTPs, referred as DWTP-1 and DWTP-2. The two SSFs receive water from the same source after the same pre-treatment processes. Generally, the raw water, withdrawn from the river near Brakel and purified through sand filters, is transported through two pipes to the dunes located between DWTP-1 and DWTP-2. After the infiltration in the dunes and an average residence time of two months, the water is pumped up for a series of post-treatment steps before being transported to customers; these steps include softening, aeration with preliminary dosing of powdered activated carbon, dual media rapid filtration, and SSF. During the operation, the top layers of SSFs are removed to control the head loss over the filters. Typically, the top ~10 cm of filter material, including the SCM layer, are removed. Subsequently, the scrapped sand is washed, dried, and then reused. The two dimensionally distinct SSFs have been used for drinking water production at DWTP-1 and DWTP-2 since 2006 and 1999. Both of the SSFs are covered. The characteristics of the SSFs are shown in Table S1.

2.2. Sample collection

The schematic representation of the sampling of the SSFs is shown in Figure S1. Both of the SSFs were sampled near terminal head loss when the SCMs were most developed. All of the samples taken were stored in sterile plastic containers on ice and analyzed within 24 h.

For biomass quantification, triplicate samples from the SCM-10 cm top layers of SSFs were collected immediately after the SSFs were drained out. The SCM layers (dark black) were distinguishable from the sand bed (dark brown) by their color, which were biofilm-like layers accumulated on the top of sand filter bed (Campos et al., 2002). Specifically, a hole was dug for sample collection. The SCM samples were collected first; then, sequentially, sand samples were collected from the depth 0–2 cm ($D_{0-2\ cm}$), 4–6 cm ($D_{4-6\ cm}$), and 8–10 cm ($D_{8-10\ cm}$) of the sand beds, using a sterile spatula ($n = 24$, triplicate samples, 4 layers, 2 filters).

The microbial community assembly study was focus on the SSF in DWTP-1, where three influent samples were collected for DNA extraction and sequencing once per week in three successive weeks (water samples, $n = 3$) before taking filter samples, and triplicate samples from each filter layer were collected for DNA extraction and sequencing (SCM and sand samples, $n = 12$, triplicate samples, 4 layers). To assess the similarity and variation of the microbial community between the two full scale SSFs in two treatment plants, 2 layers rather than all 4 layers were randomly chosen and sampled from SSF in DWTP-2 ($D_{0-2\ cm}$ and $D_{4-6\ cm}$, duplicate sand samples, $n = 4$) to be compared with that of the same depth in DWTP-1. Generally, the influent water samples (2 L per sample) were filtrated with 0.2 μm filters for DNA extraction. While, suspensions of all the SCM and sand samples, which were obtained by ultrasonification for three time periods of 2 min each at 42 KHz, were used for further microbiological analysis (Liu et al., 2018).

2.3. Active biomass concentration measurements

The active biomass concentration was determined by measuring the Adenosine triphosphate (ATP) content and intact cell counts

(ICC) in the suspensions of all the SCM and sand samples. The ATP content was measured using the Luciferene Luciferase method. In short, the obtained suspensions were warmed to 30 °C in a sterile Eppendorf tube, while the ATP reagent was simultaneously warmed. The sample and the reagent were mixed with an equal volume after 2 min at 30 °C and then the luminescence was measured directly. The data were collected as relative light units and converted to ATP by means of a calibration curve made with a known ATP standard (BactTiter kit, Promega, method detection limit 0.5 ng/L). Total intact cell counts were determined through flow cytometry (FCM, BD Accuri C6® FCM, BD Biosciences, Belgium). SYBR Green I and Propidium Iodide was used to distinguish living and dead cells (Chan et al., 2018). In detail, bacterial cells in the suspensions (500 μL per sample) were stained with 5 μL of the mixture of SYBR® Green I and propidium iodide stains and incubated for 15 min in the dark before measurement.

2.4. DNA extraction and illumina sequencing

The DNA was extracted from the water samples and the suspensions of all the SCM and sand samples using the FastDNA Spin Kit for Soil (Q-Biogene/MP Biomedicals, Solon, OH, USA), following the manufacturer's instructions (Hwang et al., 2011; Tamaki et al., 2011). The 16S rRNA gene amplification was carried out as previously described (Kozich et al., 2013). The hypervariable V3—V4 region of the 16S rRNA gene was amplified with the bacterium-specific forward primer 341F (5′-CCTACGGGNGGCWGCAG-3′) and the reverse primer 805R (5′-GACTACHVGGGTATCTAATCC-3′). The sequencing was performed on the Illumina Life Sciences GS FLX series genome sequencer (Roche, Switzerland). The obtained DNA sequences were deposited in the DDBJ sequence read archive (Accession Number: PRJNA643380).

2.5. Statistical analysis

The raw reads generated were filtered, clustered, and aligned using the Quantitative Insights Into Microbial Ecology (QIIME2) pipeline with default settings (Kuczynski et al., 2011). Taxonomy assignment against the bacterial SILVA database were performed. Additionally, all samples were rarefied to the lowest read number within the data set (7,000) for the downstream alpha and beta diversity analysis. Dissimilarity across samples was calculated by using unweighted UniFrac distance matrices, which were constructed from the phylogenetic tree and exhibited by the principal coordinate analysis (PCoA) plot. The significance of beta diversity differences among different sample categories was determined by the PERMANOVA test in QIIME2. Differences were considered significant when the p-value was lower than 0.05 ($p < 0.05$). Venn diagrams exhibiting the similarity of the microbial populations among distinct sample categories were drawn with VennDiagram package in R (3.5.3). The least discriminant analysis (LDA) effect size (LEfSe) was performed to distinguish biomarker taxa with significantly different relative abundances ($P < 0.05$, LDA score > 2) in each group.

To explore the contribution of neutral processes and environmental selection on community assembly of the filter communities, an evolved NCM following null hypothesis was performed (Morris et al., 2013). Specifically, the influent water sample was considered to be the source community, whereas the filter media samples, including the SCM layer and sand samples, were the local target communities. The empirically observed frequency of detection was expressed as the number of filter media samples, in which a target OTU was detected over the total number of filter media samples. In the implementation of this model, only shared OTUs between target and source communities were employed. Consequently, the expected frequency of detection in the target communities, which were present via dispersal and ecological drift, was calculated following a beta probability distribution (Sloan et al., 2006). The probability distribution was estimated by the coupled parameter N_Tm and the relative abundance of the OTU in the source community. Wherein, N_T represents the total number of individuals in the local community, and m is the immigration rate. The fitting parameter N_Tm, which reflects the dispersal of microbes from the source community to the target community, was optimized by minimizing the sum of squares of errors. Ultimately, the neutral model was constructed by 95% binomial confidence intervals based on the Wilson method with the Hmisc package in R (Morris et al., 2013). Theoretically, OTUs that fell between the confidence intervals were considered to be a result of neutral dynamics of stochastic births and deaths within the local communities and stochastic immigration from the source communities, according to the neutrality assumption. OTUs falling outside the upper or lower bound of the confidence interval were detected at disproportionately higher or less frequencies in the local communities than predicted by the neutral model, based on their relative abundance in the source communities, which are advantaged or disadvantaged by the local environment (Vignola et al., 2018).

2.6. Functional assignment and analysis

The functional potential of prokaryotic communities in all samples was predicted using Phylogenetic Investigation of Communities by Reconstruction of Unobserved States (PICRUSt) v1.0.0 pipeline. Sequences used for PICRUSt were clustered at 97% similarity using the *pick_closed_reference_otus.py* script against the 13.5 Greengenes database on QIIME platform (Langille et al., 2013; Wang et al., 2016). The OTU table normalized by 16S rRNA gene copy number was used for metagenome functional prediction, generating a table of Kyoto Encyclopedia of Genes and Genomes (KEGG) Orthologs (KOs). Ultimately, the predicted functions were categorized at KO level 2 and 3 within the pathway hierarchy of KEGG. The Nearest Sequenced Taxon Index (NSTI) score, an indicator for the accuracy of PICURSt, was generated by using default settings (Langille et al., 2013). The comparison of potential functions among different sample categories were completed using statistical analysis of metagenomic profiles (STAMP). All possible pairwise Spearman's rank correlations between bacterial taxa and predicted metabolic sub-pathways were calculated, and a correlation matrix was constructed in R environment using psych package. A valid co-occurrence event was considered to be a robust correlation if the Spearman's correlation coefficient (ρ) was >0.7 and statistically significant (P-value <0.01) (Barberan et al., 2012). Gephi 0.9.1 was used for network visualization (Bastian et al., 2009).

3. Results

3.1. Biomass distribution along filter depth

As quantified by ATP and ICC, the SCM harbored the highest active biomass (1.1—1.9 × 10^9 cells g^{-1}, 80.1—154.1 ng ATP g^{-1}). For both DWTPs, the biomass distribution showed the same trend along depth; the biomass decreased sharply from the SCM to $D_{0-2\ cm}$, then gradually to $D_{4-6\ cm}$ and $D_{8-10\ cm}$. In the SSF of DWTP-1, ATP decreased by 50%, 67%, and 75%, and ICC decreased by 91%, 96%, and 97%, from the SCM to $D_{0-2\ cm}$, $D_{4-6\ cm}$, and $D_{8-10\ cm}$, respectively (Fig. 1). For DWTP-2, ATP decreased by 85%, 91%, 94%, and ICC decreased by 90%, 94%, 95%, from the SCM to $D_{0-2\ cm}$, $D_{4-6\ cm}$, and $D_{8-10\ cm}$, respectively (Fig. 1). It is interesting to observe that with a ~200 days longer filter-run time (450 vs. 243 days), the SCM

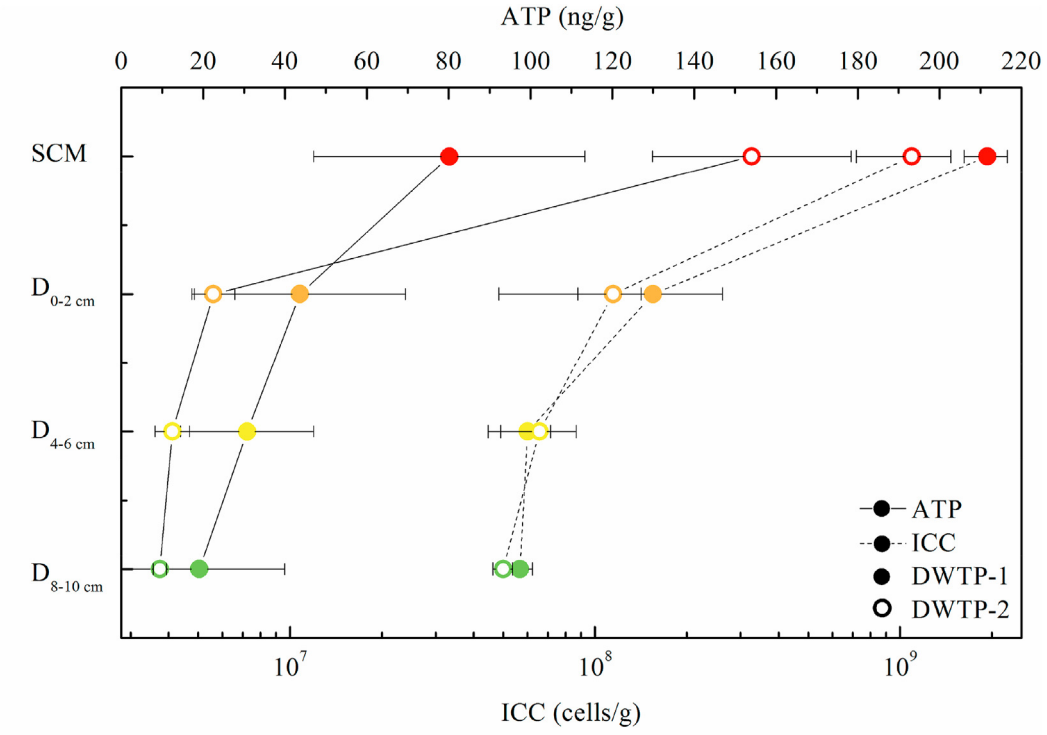

Fig. 1. The variations of ATP and intact cell counts (ICC) in Schmutzdecke (SCM, red), and sand samples with different depth ($D_{0-2\ cm}$, orange; $D_{4-6\ cm}$, yellow; $D_{8-10\ cm}$, green) in DWTP-1 and DWTP-2.

from DWTP-2 harbored much higher active biomass than that of DWTP-1 (ATP, 154.1 vs. 80.1 ng/g). While going deeper into the sand bed, the ATP of DWTP-2 became lower than that of DWTP-1 at the same depth, with much smaller differences (10–20 ng/g) compared to the differences between the SCMs.

3.2. Microbial community distribution along filter depth

In total, 263,185 sequences were obtained from 19 samples, including water samples, SCM, $D_{0-2\ cm}$, $D_{4-6\ cm}$, and $D_{8-10\ cm}$ sand samples in triplicates ($n = 15$) from DWTP-1, and selective sand samples from $D_{0-2\ cm}$ and $D_{4-6\ cm}$ in duplicate ($n = 4$) from DWTP-2, with an average number of about 13,000 reads/sample, which assigned as 1110 OTUs. The comparison of the microbial community of the different layers is based on DWTP-1, while the comparison of the two sand filters is based on $D_{0-2\ cm}$ and $D_{4-6\ cm}$. The rarefaction curve reached a plateau after 5000 sequence reads were obtained, indicating that enough sample coverage was obtained for all the samples (Figure S2). All samples were rarefied to the lowest read number within the data set (7,000) for the downstream alpha and beta diversity analysis.

3.2.1. The diversity of microbial communities

Alpha diversity. On average, 404–528 OTUs were observed across all samples (Table S2). When the two treatment plants were compared, similar levels of OTUs were observed at $D_{0-2\ cm}$ and $D_{4-6\ cm}$ between the SSFs. For the distribution of OTUs along depth, the same trend as that of the biomass distribution was observed for the number of observed OTUs, which decreased from 528 at the SCM to 502, 470, and 404 at $D_{0-2\ cm}$, $D_{4-6\ cm}$, and $D_{8-10\ cm}$, respectively. The same trend was observed for the indices of Shannon and Chao 1, while no clear differences were found regarding the evenness.

Beta diversity. PCoA plot based on UniFrac distance showed three clusters, namely: water samples, the SCM, and other layers, indicating the high reproducibility of the obtained results (replicates), and the clear differences among sample groups of water, the SCM, and the sands (PERMANOVA, $p < 0.01$) (Fig. 2). Remarkably, the sand samples from layers of $D_{0-2\ cm}$ and $D_{4-6\ cm}$ of the two treatment plants clustered closely together (PERMANOVA, $p > 0.05$), suggesting identical bacterial community formation in the SSFs, despite the differences of the locations and operational conditions of the two treatment plants. Considering the microbial community distribution along depth, the SCM formed a different cluster from all other sand samples (PERMANOVA, $p < 0.01$). One of the sand samples from $D_{0-2\ cm}$ in DWTP-1 showed bigger variations among the triplicate samples than did all the others; the sample was taken from the upper part of the sand connecting to the SCM as reflected by a closer distance to the cluster of SCM in the PCoA plot.

3.2.2. The composition of the microbial communities

The taxonomy assignment showed that at the phylum level, Proteobacteria (22.2–34.5%) and Planctomycetes (14.1–18.3%) were highly abundant in filter samples, while Patescibacteria (36.0%), Proteobacteria (20.2%) and Omnitrophicaeota (14.0%) dominated in water samples (Figure S3). Not all OTUs were able to be assigned into known general taxonomy information due to the complexity in the microbial community within this oligotrophic environment. As shown in Fig. 3A and Figure S4, OTU52 (c_Subgroup 6, 3.1–4.1%), OTU607 (f_Gemmataceae, 2.6–3.6%), and OTU859 (o_PLTA13, 2.1–3.8%) were the most abundant taxa in the sand samples of the top layers, followed by OTU860 (*Pseudomonas* spp., 0–3.0%), OTU820 (MND1 spp., 0.9–2.8%), OTU668 (*Pedomicrobium* spp., 0.7–2.4%), OTU357 (*Nitrospira* spp., 1.2–2.1%), OTU613 (f_Pirellulacea, 1.3–2.5%), OTU873 (*Methylomirabilis* spp., 0.9–1.8%), OTU575 (c_OM190, 1.0–1.8%), OTU610 (*Pir4 lineage* spp., 1.3–1.7%), OTU827 (f_TRA3-20, 0.4–1.7%), OTU223 (o_S085, 0.9–1.3%),

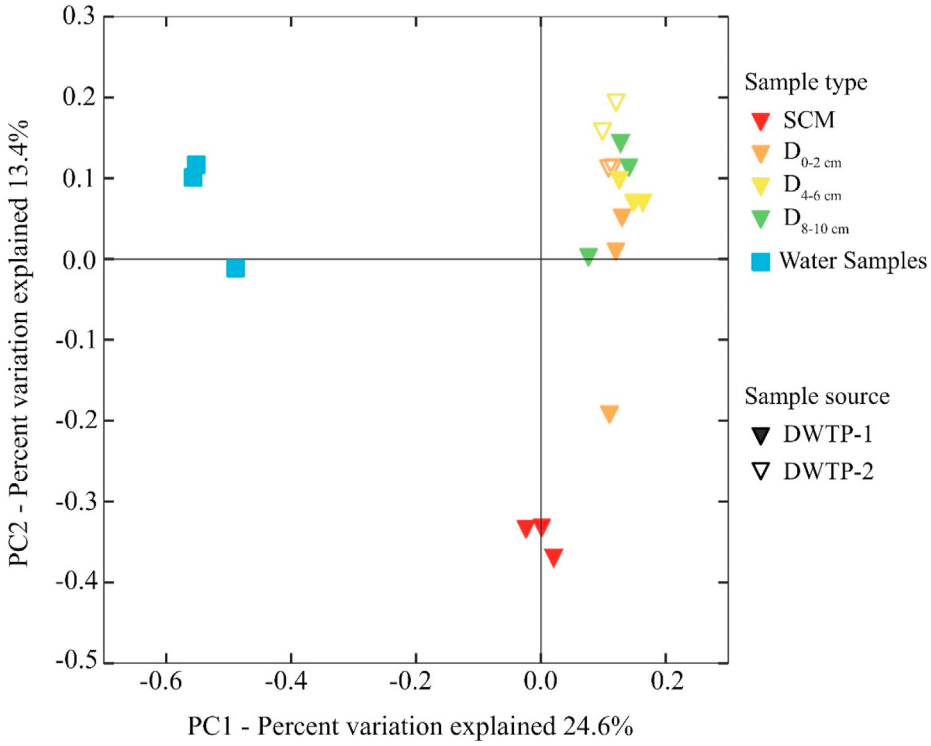

Fig. 2. PCoA plot generated using unweighted UniFrac distance matrix showing the microbial community distribution of different sample categories.

OTU850 (*Legionella* spp., 0.3−1.3%), OTU247 (c_TK10, 0.2−1.3%), and OTU667 (*Hyphomicrobium* spp., 0−1.3%), OTU611 (*Pirellula* spp., 0.8−1.2%), OTU732 (o_MBNT15, 0.7−1.2%), OTU680 (f_Xanthobacteraceae, 0−1.2%), OTU196 (*Anaerolineaceae* spp., 0.1−1.1%), and OTU130 (f_Saprospiraceae, 0.3−1.1%).

Along the depth of the filter bed, there were 66 dominant OTUs (>1%) shared by all layers (93 dominant OTUs), of which OTU52, OTU607, OTU859, and OTU613 accounted for the highest abundances in the SCM, $D_{0-2\ cm}$, $D_{4-6\ cm}$, and $D_{8-10\ cm}$, respectively (Figure S5). In addition, significantly different dominant OTUs between the SCM and other top sand layers were observed (Fig. 3B). For example, 9 dominant OTUs (>1%) were discriminatively dominant in SCM (Welch's *t*-test, two-sided, Bonferroni method, 95% confidence interval, $p < 0.05$), namely, OTU668, OTU873, OTU667, OTU850, OTU680, OTU196, OTU130, OTU645 and OTU666 in descending order, while for the top 10 cm of the sand layers, OTU820, OTU613, OTU357, OTU860, OTU827, OTU732, OTU611, OTU247, OTU711, OTU235, OTU184, OTU178, and OTU561 were discriminatively dominant (Welch's *t*-test, two-sided, Bonferroni method, 95% confidence interval, $p < 0.05$) (Fig. 3B). However, among the three studied top sand layers ($D_{0-2\ cm}$, $D_{4-6\ cm}$ and $D_{8-10\ cm}$), hardly any discriminative dominant OTUs were found (Figure S6). The detailed taxonomy information of above-mentioned OTUs was shown in Figure S4.

In the water phase, OTU372 (f_Omnitrophicaeota, 6.4%) was the most abundant taxa, followed by OTU446 (o_JGI 0000069-P22, 3.2%), OTU552 (c_Parcubacteria, 2.2%), OTU879 (o_Rokubacteriales, 2.0%), OTU365 (*Candidatus Omnitrophus* spp., 2.0%), OTU52 (1.3%), and OTU827 (1.1%).

3.3. Effects of neutral processes on filter microbial community assembly

According to modified NCM, there was a weak correlation between the neutral model prediction and the empirical observations (Spearman rank correlation coefficient = 0.15, $p < 0.05$, Fig. 4). Among the 248 shared OTUs between microbes in the influents and the filter bed, 48.4% of OTUs can be explained by neutral process, while 51.6% OTUs were either more frequent (27.4%) or less frequent (24.2%) than would be expected by their relative abundances if neutral processes dominated microbial community assembly. When the weight of sequences for each OTU was taken into consideration, the neutral process still explained about 44.8% of the sequences, but the enriched OTUs' contribution increased to 50%, and the disadvantaged OTUs' contribution decreased to 5.2% (Table S3). When zooming into different layers along the depth (Table S4 and Figure S7), the neutral model failed to explain microbial community assembly in the layers of the SCM, $D_{0-2\ cm}$ and $D_{4-6\ cm}$, while weak correlation was observed for $D_{8-10\ cm}$, indicating that environmental selection influences the top sand layers.

The OTUs with observed frequencies above, below, or within 95% confidence intervals of NCM prediction, were identified and defined as enriched, disadvantaged, and neutral OTUs, respectively. Thirteen dominant OTUs (>1%) fell into the category of enriched OTUs, including OTU820, OTU613, OTU610, OTU575, OTU611, OTU645, OTU142, OTU711, OTU247, OTU235, OTU178, OTU561, and OTU130, in descending order. Among the 60 disadvantaged OTUs, the relative abundance of dominant OTUs decreased significantly (i.e., OTU372, OTU552, OTU369, OTU444, OTU549, OTU365, and OTU879) (decreased by 88%−99%). For the neutral developed groups, there were 11 dominant OTUs (i.e., OTU52, OTU607, OTU357, OTU668, OTU873, OTU827, OTU184, OTU850, OTU196, OTU667, and OTU680). It should also be mentioned that the unique OTUs observed in filter communities but not in the influents accounted for an unignored abundance (356 OTUs, 42%), which were dominated by OTU859, OTU860, OTU223, OTU679, OTU732, and OTU666 (>1%). The taxonomic information of above-mentioned OTUs was given in Figure S4.

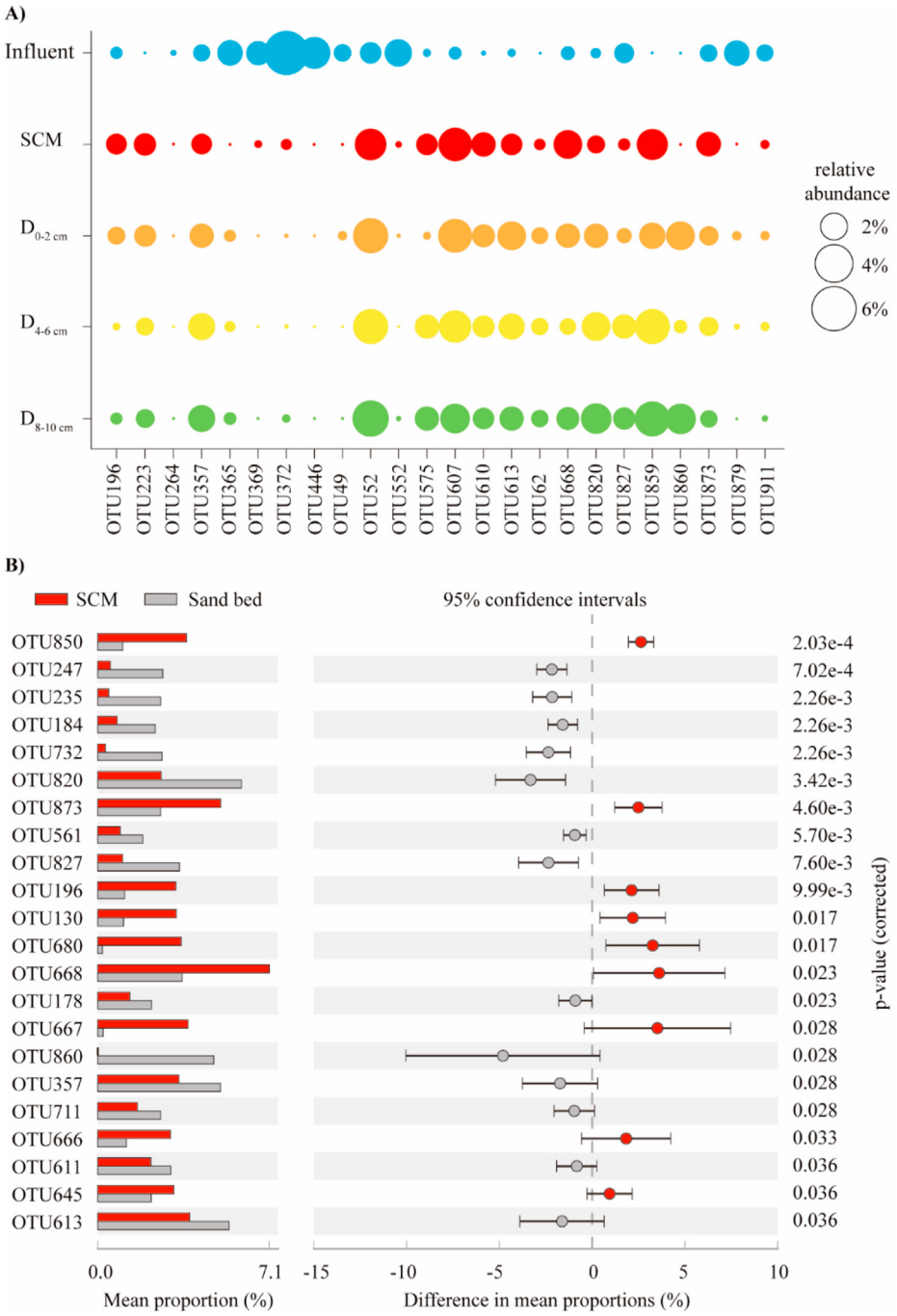

Fig. 3. A) Heatmap showing the core OTUs (relative abundance >2%) and their relative abundance in all samples. The complete list of dominant OTUs (relative abundance >1%) and their relative abundance in all samples was shown in Figure S3. B) Extended error bar plot identifying significant differences between mean proportions of dominant OTUs in SCM (red) and sand bed (0–2 cm, 4–6 cm, 8–10 cm of the sand, gray) samples. The plot was generated in STAMP (Welch's *t*-test, two-sided, Bonferroni method, 95% confidence interval, $p < 0.05$).

3.4. The distribution of predicted metabolic functions along depth

In total, PICRUSt generated 5938 predicted metagenomes based on 16S rRNA gene amplicon data sets, which collapsed into 41 and 234 functional pathways at levels 2 and 3 using KEGG pathway metadata. With NSTI scores of 0.23 ± 0.02, the predicted functional pathways are authentic (Table S5). Specifically, membrane transport affiliated to environmental information processing, amino acid metabolism, and carbohydrate metabolism were the most abundant pathways (>10%) at level 2 in the studied top layers (Fig. 5). At level 3, there were 35 dominant predicted functions (>1%), among which transporters and ABC transporters affiliated to membrane transport accounted for the highest abundances (Figure S8).

When the predicted functions between the SCM and the other top sand layers were compared, significant differences were observed (Figure S9 and S10). In the SCM, a broad range of metabolisms were significantly more abundant than in the top sand layers, such as genes related to the metabolism of porphyrin, chlorophyll, butanoate, propanoate, nitrogen, linoleic acid, cytochrome P450, xenobiotic, D-Alanine, the degradation of

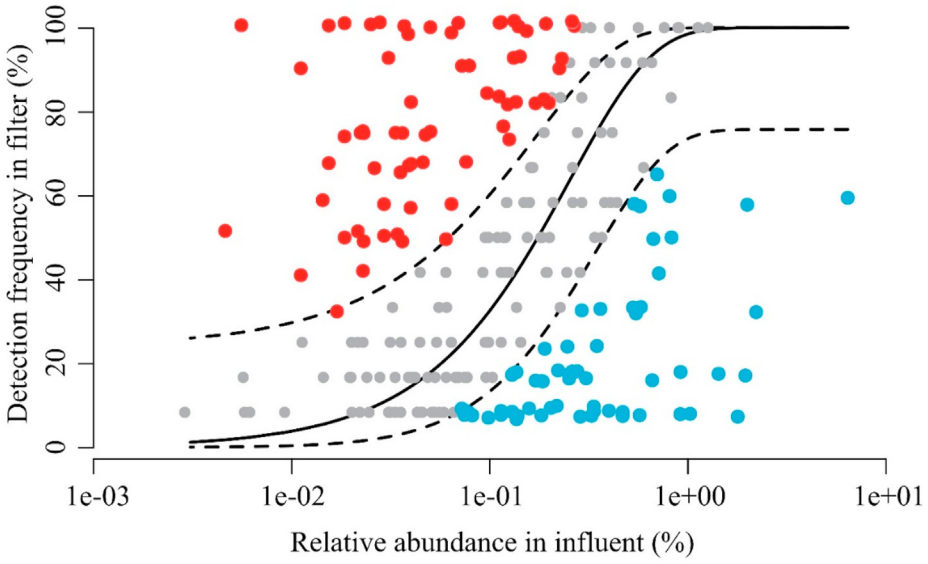

Fig. 4. Neutral community model for the uppermost filter samples. The solid line is the model prediction and dashed lines represent 95% confidence intervals. Red points represent the OTUs for which the observed frequency is greater than the model prediction (enriched), and blue points represent the OTUs for which the observed frequency is less than the prediction (disadvantaged), based on their mean relative abundance in the influent communities.

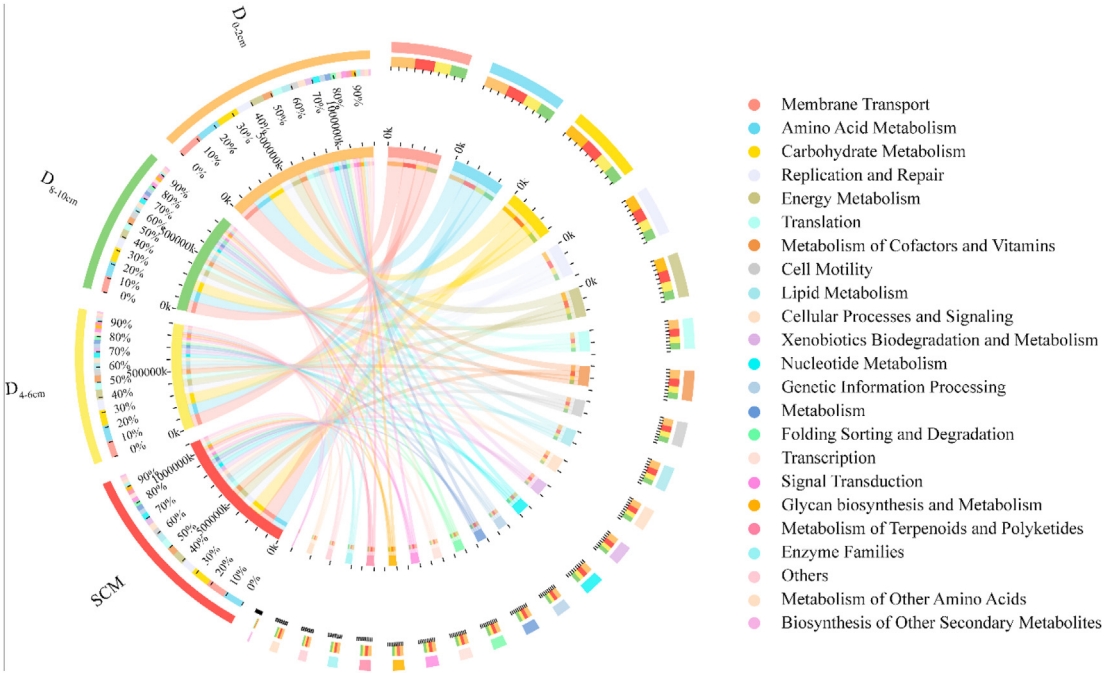

Fig. 5. The distribution of metabolic functions along depth at KEGG level 2. The left half of the circle shows the sample categories, whereas the right half of the circle shows the metabolic functions at KEGG level 2. The thickness of each ribbon represents the abundance of each metabolic functions.

chloroalkane, chloroalkene, and bisphenol, and the photosynthesis of proteins ($p < 0.01$) (Figure S10). For the top sand layers, genes associated with the metabolism of carbohydrate, nicotinate, nicotinamide, glycosaminoglycan, glycerophospholipid, and arachidonic acid, the biosynthesis of penicillin and cephalosporin, and the degradation of xylene were significantly more abundant ($p < 0.01$). While going deeper into the sand, genes linked to the metabolism of amino acid, nicotinate, nicotinamide, and phosphonate, the degradation of glycosaminoglycan, the biosynthesis of phenylalanine, tyrosine and tryptophan, DNA repair and recombination proteins were most abundant in $D_{4-6\ cm}$ ($p < 0.01$) (Figure S11B); while genes related to fructose and mannose metabolism and other transporters were most abundant in $D_{0-2\ cm}$ and $D_{8-10\ cm}$ ($p < 0.01$) (Figure S11A and S11C).

3.5. The co-occurrence patterns between dominant OTUs and predicted functions

Co-network analysis visualized the co-occurrence patterns of dominant OTUs (>1%) that colonized the filter and predicted functions at Level 3 in all samples (Figure S12). 67 positive correlations were established among 18 OTUs and 44 metabolic

functions. The 18 dominant OTUs (>1%) involved in the network analysis were composed of 7 enriched OTUs according to NCM (i.e., OTU820, OTU613, OTU611, OTU711, OTU247, OTU561, and OTU130), 6 neutral OTUs (i.e., OTU607, OTU357, OTU184, OTU850, OTU667, OTU680), and 5 unique OTUs (i.e., OTU859, OTU860, OTU666, OTU679, OTU732). Detailed correlations between predicted functions and bacterial taxa were provided in Table S6.

4. Discussion

We studied the top 10 cm of full-scale SSFs layer by layer (every ~2 cm) in two drinking water treatment plants that received the same artificial recharged groundwater as source water. The triplicate samples from each full-scale filter bed and the replicated filter beds from the two treatment plants confirmed the high reproducibility and reliability of the obtained results. Though SSFs have been widely documented, this work sheds new light on the differences in active biomass, the assembly of communities, and the shifts of metabolic functions from the SCM to 10 cm below the surface of the sand beds. To the best of our knowledge, this is the first study to integrate quantity, community, and metabolic function datasets, providing details of variations at centimeter level to reveal the microbial ecology of full-scale SSFs for drinking water purification.

4.1. Bioactive top layers of SSFs for drinking water purification

As revealed by ICC and ATP results, both the biomass and bioactivity decreased as the depth increased, from the SCM to the sand beds, in both of the treatment plants. This agrees with the general trends reported previously for rapid and SSFs (Campos et al., 2002; Nitzsche et al., 2015; Carpenter and Helbling, 2017). For example, using untreated reservoir water as a source and treating it for irrigation purposes, Calvo-Bado et al. observed similar levels of ATP (129 ng/g) on the surface of the sand bed, which decreased to 3.6 ng/g and remained stable at 3.8 ng/g at the middle (50 cm) and bottom (100 cm) of a 1-m deep simulated slow sand filter bed (Calvo-Bado et al., 2003). In a similar sampling program of every 2 cm for the top 10 cm, Campos et al. observed a different trend, in which, after 69 days operation, the biomass differences between the layers in the SSFs not exposed to sunlight were not significant; this was quantified by extractable organic carbon fraction released from the lysis of microbial cells by chloroform fumigation (Campos et al., 2002). The different trends between the observations of Campos et al. and other studies (including the present one) might be caused by a short operation time (69 vs. 243, 450 days), or the different ways of quantifying the biomass (chloroform fumigation vs. cells, ATP). It has been reported that chloroform gas may adsorb significantly to some fractions of soil causing uncertainties, which could be the case for EPS and other components in the SSFs (Alessi et al., 2011).

Remarkably, the layer-by-layer, centimeter-scale analysis of the SSFs in both treatment plants highlighted that the sharpest decrease in active biomass occurred between the SCM and the sand bed, where ATP decreased by 50−85% and ICC decreased by >90%. There was only a slight additional decrease in the top 4 cm of the sand bed, and ATP and ICC remained stable deeper into the sand bed. This indicates that the SCM is a very bioactive layer for contaminant degradation, which echoes previous studies that attributed the biological removal of a wide range of organic matter to the SCM (Oh et al., 2018). When the two SSFs were compared, the ATP in the SCMs was positively correlated with operation time, that is, the SCM is more bioactive for organic nutrient and contaminant degradation after 450 days than after 243 days. The higher ATP can be attributed to its longer operation time and more flux, during the period of which the filtrated water kept delivering nutrients to SCM for microbial growth.

Moreover, it is interesting to observe that the higher ATP in the SCM after 450 days' operation decreased more sharply to sand bed than that of the 243 days' operation (85% vs. 50%), which, on the contrary, resulted in lower ATP in all layers in the longer operated sand bed. This observation is a direct proof that the more bioactive SCM degraded more organic matter (better purification performance), leading to the lower ATP downstream deeper in the sand bed. However, the SCM is also responsible for the head loss over sand filters (Campos et al., 2002). To achieve the optimized performance of SSFs, the activity for biodegradation and the level of head loss should be balanced.

4.2. Microbial community and metabolic functions

Despite differences in operation time and treatment plant location, the microbial communities of the SSFs top layers in the two treatment plants were very similar, suggesting the minor influence of these factors (operation time and plant location) on shaping matured microbial communities in SSFs. Similarly, Haig et al. found that the type and location of filters was not significant in explaining microbial community variations, when assessing mature samples in industrial or laboratory-scale SSFs that received the same source water (Haig et al., 2014). This might be because the microbial community in filters depends on the nutrient composition of water flowing through the filters (Pinto et al., 2012); in both the present study and Haig et al., the different filters received the same water and had similar established microbial communities. Within the top layers, the high abundance of *Pedomicrobium* spp. and *Pseudomonas* spp. suggested the occurrence of mineral biodegradation (Wang et al., 2010). Besides, the co-presence of MND1 spp. that oxidize ammonia to nitrite (Prosser et al., 2014) and the nitrifying bacteria *Nitrospira* spp.(Lucker et al., 2010) indicated that the process of nitrification/denitrification took place in the top layers, which agrees with previous studies (Oh et al., 2018; Aslan and Cakici, 2007).

When the SCM and other layers of the sand bed were compared, the same trend as ATP and ICC was observed for alpha diversity indices, suggesting the highest microbial diversity in the SCM, which can be explained by the higher level of retention of both cells and organic matter. It has been reported that the higher community diversity could promote ecosystem services (Maron et al., 2018) and enhance the adaptability to water quality changes (Wittebolle et al., 2009), which indicates the high metabolic versatility and functional stability of the SCM (Haig et al., 2015), and agrees with a previous conclusion that the SCM layer is the most effective water purification compartment (Wakelin et al., 2011).

With regard to the microbial community composition, the genera *Candidatus Methylomirebilis* spp. (1.8%) and *Hyphomicrobium* spp. (1.3%) were highly enriched in the SCM, indicating the occurrence of biological denitrification within the SCM (Wang et al., 2010; Luesken et al., 2012). Moreover, other amino acids (D-Alanine metabolism) related metabolic capacities were also enriched in the SCM. In contrast, high abundance of *Pseudomonas* spp. (0.5%−3.0%) was observed in sand samples; these were able to oxidize carbohydrates (e.g. glucose) to produce exopolysaccharides for biofilm formation, and oxidize minerals (e.g. iron) (White et al., 2015; Bai et al., 2016). This is consistent with the presence of enriched carbohydrate metabolism in the sand bed.

4.3. Microbial community assembly in the top layers of SSFs

Taking influent as the source metacommunity, it was observed that the filter communities were not strongly assembled by neutral

processes, and the filter environment provided a selective environment, facilitating deterministic selection forces to overcome stochastic ones during the operation (Dini-Andreote et al., 2015). This is consistent with the previous lab study that investigated neutral and deterministic factors in the assembly of rapid sand and granular carbon filter microbial communities, and the study on microbial wastewater treatment communities (Vignola et al., 2018; Hou et al., 2019; Ofiteru et al., 2010). Moreover, when one zooms into the SCM and the different top layers in the sand bed, the communities of all other layers above were governed by environmental selection pressure, only a small portion of the community of $D_{8-10\ cm}$ layer can be weakly explained by neutral process ($P < 0.01$).

NCM categorized the community members as enriched or disadvantaged by the selection of filtration processes. In the case of filter microbial communities, the enriched taxa might be strong competitors adapting for growth in the niche of filter bed, and were most likely to be responsible for water purification. For example, the enriched OTUs (i.e., OTU610, OTU611, OTU613) assigned to the family of Pirellulaceae can use a wide variety of carbon sources (Zhang et al., 2019; Clum et al., 2009), which was confirmed by the co-occurrence patterns between these taxa and the predicted functional pathways for amino acids, carbohydrate metabolism, glycan biosynthesis, and metabolism (Figure S12). In contrast, the disadvantaged taxa are probably the ones that cannot easily form biofilm on sand surfaces, or the weak competitors in the biofilm passed through the filter, or the ones predated by eukaryotic bacterivores (Langenheder and Jurgens, 2001).

The presence of the neutrally distributed taxa depended largely on the corresponding relative abundance in the source metacommunity, which does not mean that the functions of these taxa are insignificant. The highly abundant neutral distributors (e.g. OTU357, assigned as *Nitrospira* spp.; OTU667, assigned as *Hyphomicrobium* spp.) could be the colonizers, which are able to easily adhere and multiply on the filter medium, forming a dense biofilm structure (Luhrig et al., 2015). This hypothesis was directly evidenced by the observation of high correlations between the dominant neutrally distributed taxa (OTU357) and the predicted functional pathways related to cell motility (e.g. bacterial motility proteins, flagellar assembly) (Figure S12) (Picioreanu et al., 2007). Together with extracellular polymeric substance, biofilm developed in the filter is responsible for biotransformation and removal of contaminants (e.g. assimilation, oxidization, and degradation) (Vries et al., 2017).

In addition, there is another group of non-negligible microbial consortia with a considerable abundance, which was only detected in the filter communities, but not in the influent. These unique OTUs could be derived from the growth of inherent inhabitants in the filter medium. Alternatively, those OTUs might present in the previous water samples which were not collected in the sampling period, or present in exceptionally low numbers that cannot be detected but find a niche in the filters to settle and multiply. The former case can be investigated by higher resolution water sampling, while the latter case will require attention on the function of rare groups in the development of filter microbial ecology.

4.4. Practical implications

The centimeter-resolution data revealed the distribution of microbial quantity, community, and function within the SCM and the top 10 cm of the SSFs. There is clearly an overwhelming superiority of the SCM compared to the other top layers, even to the 0–2 cm sand bed, regarding its highest microbial abundance, diversity, and broad range of functions. This confirmed the clearly essential role of the SCM in the water purification. Typically, the SCM and the top centimeters of the sand bed are removed when the bed resistance (head loss) becomes too high. Afterwards, a ripening period has to be respected to allow the SCM to re-establish; it may take up to 6–8 weeks to "culture" the new SCM and restore performance (Joubert and Pillay, 2008). The significant differences in the microbial communities in the SCM and in the top sand layers suggest that the microbes in the remaining sand bed (new surface) may not be very helpful in accelerating the formation of the new SCM. It is therefore recommended that the old SCM not be completely removed, or be partly returned to the sand filter, in order to accelerate the ripening process.

Moreover, layer by layer, we found that environmental selection governed the SCM and top sand layers to a depth of 6 cm, while neutral processes could only explain a small portion of communities at 8–10 cm. When one considers that the communities found in the same layers of the two full-scale filters from the two treatment plants were almost identical, one can conclude that the microbial communities in the filters are reproduceable, and very likely manageable. We have shown that the operation time and treatment plant location do not change the microbial communities. It would be interesting to investigate which environmental or operational parameters might drive the microbial community assembly differently. For instance, it is indicated that the existed variations within microbial communities were driven by environmental and chemical gradients (e.g., DOC, NH_4^+) (Haig et al., 2015; Boon et al., 2011). Therefore, it is possible that the dissimilarity among the communities within SCM and sand bed layers was attributed to the differences in chemical gradient distribution along with depth. Nevertheless, more efforts should be made to explore the secrets. Culturing the microbes that are key purifiers, such as those that can metabolize complex and persistent organic matter, would be helpful with a view to optimizing contaminant removal. This would be all the more meaningful given that microbes harbored by biofilters strongly contribute to the drinking water microbiome (Pinto et al., 2012).

In summary, the biomass in the filer decreased rapidly along the depth, which was most pronounced from the SCM to the surface sand layer (0–2 cm). The alpha diversity indices followed the same trend with active biomass results, suggesting more active and diverse communities in SCM. The beta diversity results concluded that the filter communities at the same depth below the sand surface in the two DWTPs clustered closely together. The SCM community was significantly different from the sand bed community, with significant over-representation of metabolism and degradation of complex organic matters (e.g., butanoate, propanoate, and bisphenol). Functional importance of SCM was further confirmed by the co-occurrence patterns of the dominant taxa/OTUs and metabolic functions. Using an island biogeography model, we found that microbial communities in SSFs were strongly assembled by selection rather than by neutral processes (e.g. mitigating from the microbial communities in the influents). We strongly recommend the environmental parameters that drive filter community assembly, especially in the SCM, to be identified in order to optimize the performance of SSFs through engineering measures.

CRediT authorship contribution statement

Lihua Chen: conducted the research, processed the data, wrote the manuscript. **Yujia Zhai:** conducted the research, processed the data, wrote the manuscript. **Ed van der Mark:** supervised and conducted the sampling, provided comments on the manuscript. **Gang Liu:** formulate the research questions, supervised the data interpretation and manuscript preparation, wrote the manuscript. **Walter van der Meer:** supervised the study, guided the data

analysis, commented on the draft and revised manuscript. **Gertjan Medema:** supervised the study, guided the data analysis, commented on the draft and revised manuscript.

Declaration of competing interest

The authors declare that they have no known competing financial interests or personal relationships that could have appeared to influence the work reported in this paper.

Acknowledgements

The authors would like to acknowledge the support from the National Key R&D program of China (2018YFE0204100), National Natural Science Foundation of China for International Cooperation and Exchange (51820105011) and the Chinese Scholarship Council (201704910877).

Appendix A. Supplementary data

Supplementary data to this article can be found online at https://doi.org/10.1016/j.jclepro.2021.126342.

References

Abu Hasan, H., Abdullah, S.R., Kofli, N.T., Kamarudin, S.K., 2012. Effective microbes for simultaneous bio-oxidation of ammonia and manganese in biological aerated filter system. Bioresour. Technol. 124, 355–363.
Alessi, D.S., Walsh, D.M., Fein, J.B., 2011. Uncertainties in determining microbial biomass C using the chloroform fumigation–extraction method. Chem. Geol. 280 (1), 58–64.
Aslan, S., Cakici, H., 2007. Biological denitrification of drinking water in a slow sand filter. J. Hazard Mater. 148 (1–2), 253–258.
Bai, Y., Chang, Y., Liang, J., Chen, C., Qu, J., 2016. Treatment of groundwater containing Mn(II), Fe(II), As(III) and Sb(III) by bioaugmented quartz-sand filters. Water Res. 106, 126–134.
Barberan, A., Bates, S.T., Casamayor, E.O., Fierer, N., 2012. Using network analysis to explore co-occurrence patterns in soil microbial communities. ISME J. 6 (2), 343–351.
Bastian, M., Heymann, S., Jacomy, M., 2009. In: Gephi: an Open Source Software for Exploring and Manipulating Networks, Third International AAAI Conference on Weblogs and Social Media, 2009.
Boon, N., Pycke, B.F., Marzorati, M., Hammes, F., 2011. Nutrient gradients in a granular activated carbon biofilter drives bacterial community organization and dynamics. Water Res. 45 (19), 6355–6361.
Calvo-Bado, L.A., Pettitt, T.R., Parsons, N., Petch, G.M., Morgan, J.A.W., Whipps, J.M., 2003. Spatial and temporal analysis of the microbial community in slow sand filters used for treating horticultural irrigation water. Appl. Environ. Microbiol. 69 (4), 2116–2125.
Campos, L.C., Su, M.F.J., Graham, N.J.D., Smith, S.R., 2002. Biomass development in slow sand filters. Water Res. 36 (18), 4543–4551.
Carpenter, C.M.G., Helbling, D.E., 2017. Removal of micropollutants in biofilters: hydrodynamic effects on biofilm assembly and functioning. Water Res. 120, 211–221.
Chan, S., Pullerits, K., Riechelmann, J., Persson, K.M., Rådström, P., Paul, C.J., 2018. Monitoring biofilm function in new and matured full-scale slow sand filters using flow cytometric histogram image comparison (CHIC). Water Res. 138, 27–36.
Clum, A., Tindall, B.J., Sikorski, J., Ivanova, N., Mavrommatis, K., Lucas, S., Glavina, T., Del, R., Nolan, M., Chen, F., Tice, H., Pitluck, S., Cheng, J.F., Chertkov, O., Brettin, T., Han, C., Detter, J.C., Kuske, C., Bruce, D., Goodwin, L., Ovchinikova, G., Pati, A., Mikhailova, N., Chen, A., Palaniappan, K., Land, M., Hauser, L., Chang, Y.J., Jeffries, C.D., Chain, P., Rohde, M., Goker, M., Bristow, J., Eisen, J.A., Markowitz, V., Hugenholtz, P., Kyrpides, N.C., Klenk, H.P., Lapidus, A., 2009. Complete genome sequence of Pirellula staleyi type strain (ATCC 27377). Stand Genomic Sci 1 (3), 308–316.
Dini-Andreote, F., Stegen, J.C., van Elsas, J.D., Salles, J.F., 2015. Disentangling mechanisms that mediate the balance between stochastic and deterministic processes in microbial succession. Proc. Natl. Acad. Sci. U. S. A. 112 (11), E1326–E1332.
Grace, M.A., Healy, M.G., Clifford, E., 2016. Performance and surface clogging in intermittently loaded and slow sand filters containing novel media. J. Environ. Manag. 180, 102–110.
Haig, S.J., Collins, G., Davies, R.L., Dorea, C.C., Quince, C., 2011. Biological aspects of slow sand filtration: past, present and future. Water Sci. Technol. Water Supply 11 (4), 468–472.
Haig, S.J., Quince, C., Davies, R.L., Dorea, C.C., Collins, G., 2014. Replicating the microbial community and water quality performance of full-scale slow sand filters in laboratory-scale filters. Water Res. 61, 141–151.
Haig, S.J., Quince, C., Davies, R.L., Dorea, C.C., Collins, G., 2015. The relationship between microbial community evenness and function in slow sand filters. mBio 6 (5), e00729, 15.
Haig, S.J., Gauchotte-Lindsay, C., Collins, G., Quince, C., 2016. Bioaugmentation mitigates the impact of estrogen on coliform-grazing Protozoa in slow sand filters. Environ. Sci. Technol. 50 (6), 3101–3110.
Hou, L., Mulla, S.I., Nino-Garcia, J.P., Ning, D., Rashid, A., Hu, A., Yu, C.P., 2019. Deterministic and stochastic processes driving the shift in the prokaryotic community composition in wastewater treatment plants of a coastal Chinese city. Appl. Microbiol. Biotechnol. 103 (21–22), 9155–9168.
Hwang, C., Ling, F., Andersen, G.L., Lechevallier, M.W., Liu, W.T., 2011. Evaluation of methods for the extraction of DNA from drinking water distribution system biofilms. Microb. Environ. 27 (1), 9–18.
Joubert, E.D., Pillay, B., 2008. Visualisation of the microbial colonisation of a slow sand filter using an Environmental Scanning Electron Microscope. Electron. J. Biotechnol. 11 (2), 119–125.
Kozich, J.J., Westcott, S.L., Baxter, N.T., Highlander, S.K., Schloss, P.D., 2013. Development of a dual-index sequencing strategy and curation pipeline for analyzing amplicon sequence data on the MiSeq Illumina sequencing platform. Appl. Environ. Microbiol. 79 (17), 5112–5120.
Kuczynski, J., Stombaugh, J., Walters, W.A., Gonzalez, A., Caporaso, J.G., Knight, R., 2011. Using QIIME to analyze 16S rRNA gene sequences from microbial communities. Curr Protoc Bioinformatics (Chapter 10), Unit 10 7.
Langenheder, S., Jurgens, K., 2001. Regulation of bacterial biomass and community structure by metazoan and Protozoan predation. Limnol. Oceanogr. 46 (1), 121–134.
Langille, M.G., Zaneveld, J., Caporaso, J.G., McDonald, D., Knights, D., Reyes, J.A., Clemente, J.C., Burkepile, D.E., Vega Thurber, R.L., Knight, R., Beiko, R.G., Huttenhower, C., 2013. Predictive functional profiling of microbial communities using 16S rRNA marker gene sequences. Nat. Biotechnol. 31 (9), 814–821.
Li, X.-k., Chu, Z.-r., Liu, Y.-j., Zhu, M.-t., Yang, L., Zhang, J., 2013. Molecular characterization of microbial populations in full-scale biofilters treating iron, manganese and ammonia containing groundwater in Harbin, China. Bioresour. Technol. 147, 234–239.
Liu, G., Zhang, Y., van der Mark, E., Magic-Knezev, A., Pinto, A., van den Bogert, B., Liu, W., van der Meer, W., Medema, G., 2018. Assessing the origin of bacteria in tap water and distribution system in an unchlorinated drinking water system by SourceTracker using microbial community fingerprints. Water Res. 138, 86–96.
Lucker, S., Wagner, M., Maixner, F., Pelletier, E., Koch, H., Vacherie, B., Rattei, T., Damste, J.S., Spieck, E., Le Paslier, D., Daims, H., 2010. A Nitrospira metagenome illuminates the physiology and evolution of globally important nitrite-oxidizing bacteria. Proc. Natl. Acad. Sci. U. S. A. 107 (30), 13479–13484.
Luesken, F.A., Wu, M.L., Op den Camp, H.J., Keltjens, J.T., Stunnenberg, H., Francoijs, K.J., Strous, M., Jetten, M.S., 2012. Effect of oxygen on the anaerobic methanotroph 'Candidatus Methylomirabilis oxyfera': kinetic and transcriptional analysis. Environ. Microbiol. 14 (4), 1024–1034.
Luhrig, K., Canback, B., Paul, C.J., Johansson, T., Persson, K.M., Radstrom, P., 2015. Bacterial community analysis of drinking water biofilms in southern Sweden. Microb. Environ. 30 (1), 99–107.
Manav Demir, N., Atci, E.B., Demir, S., Karadeniz, A., 2018. Investigating biomass formations at different depths in a slow sand filter. Pol. J. Environ. Stud. 27 (4), 1463–1474.
Maron, P.A., Sarr, A., Kaisermann, A., Leveque, J., Mathieu, O., Guigue, J., Karimi, B., Bernard, L., Dequiedt, S., Terrat, S., Chabbi, A., Ranjard, L., 2018. High microbial diversity promotes soil ecosystem functioning. Appl. Environ. Microbiol. 84 (9).
Martineau, C., Mauffrey, F., Villemur, R., 2015. Comparative analysis of denitrifying activities of Hyphomicrobium nitrativorans, Hyphomicrobium denitrificans, and Hyphomicrobium zavarzinii. Appl. Environ. Microbiol. 81 (15), 5003–5014.
Morris, A., Beck, J.M., Schloss, P.D., Campbell, T.B., Crothers, K., Curtis, J.L., Flores, S.C., Fontenot, A.P., Ghedin, E., Huang, L., Jablonski, K., Kleerup, E., Lynch, S.V., Sodergren, E., Twigg, H., Young, V.B., Bassis, C.M., Venkataraman, A., Schmidt, T.M., Weinstock, G.M., Lung, H.I.V.M.P., 2013. Comparison of the respiratory microbiome in healthy nonsmokers and smokers. Am. J. Respir. Crit. Care Med. 187 (10), 1067–1075.
Nair, A.T., Ahammed, M.M., Davra, K., 2014. Influence of operating parameters on the performance of a household slow sand filter. Water Sci. Technol. Water Supply 14 (4), 643–649.
Nitzsche, K.S., Weigold, P., Losekann-Behrens, T., Kappler, A., Behrens, S., 2015. Microbial community composition of a household sand filter used for arsenic, iron, and manganese removal from groundwater in Vietnam. Chemosphere 138, 47–59.
Ofiteru, I.D., Lunn, M., Curtis, T.P., Wells, G.F., Criddle, C.S., Francis, C.A., Sloan, W.T., 2010. Combined niche and neutral effects in a microbial wastewater treatment community. Proc. Natl. Acad. Sci. U. S. A. 107 (35), 15345–15350.
Oh, S., Hammes, F., Liu, W.-T., 2018. Metagenomic characterization of biofilter microbial communities in a full-scale drinking water treatment plant. Water Res. 128, 278–285.
Picioreanu, C., Kreft, J.U., Klausen, M., Haagensen, J.A., Tolker-Nielsen, T., Molin, S., 2007. Microbial motility involvement in biofilm structure formation–a 3D modelling study. Water Sci. Technol. 55 (8–9), 337–343.
Pinto, A.J., Xi, C., Raskin, L., 2012. Bacterial community structure in the drinking water microbiome is governed by filtration processes. Environ. Sci. Technol. 46

(16), 8851–8859.
Pompei, C.M.E., Ciric, L., Canales, M., Karu, K., Vieira, E.M., Campos, L.C., 2017. Influence of PPCPs on the performance of intermittently operated slow sand filters for household water purification. Sci. Total Environ. 581–582, 174–185.
Prenafeta-Boldu, F.X., Trillas, I., Vinas, M., Guivernau, M., Caceres, R., Marfa, O., 2017. Effectiveness of a full-scale horizontal slow sand filter for controlling phytopathogens in recirculating hydroponics: from microbial isolation to full microbiome assessment. Sci. Total Environ. 599–600, 780–788.
Prosser, J.I., Head, I.M., Stein, L.Y., 2014. The family nitrosomonadaceae. In: The Prokaryotes, pp. 901–918.
Seeger, E.M., Braeckevelt, M., Reiche, N., Müller, J.A., Kästner, M., 2016. Removal of pathogen indicators from secondary effluent using slow sand filtration: optimization approaches. Ecol. Eng. 95, 635–644.
Sloan, W.T., Lunn, M., Woodcock, S., Head, I.M., Nee, S., Curtis, T.P., 2006. Quantifying the roles of immigration and chance in shaping prokaryote community structure. Environ. Microbiol. 8 (4), 732–740.
Tamaki, H., Wright, C.L., Li, X., Lin, Q., Hwang, C., Wang, S., Thimmapuram, J., Kamagata, Y., Liu, W.T., 2011. Analysis of 16S rRNA amplicon sequencing options on the roche/454 next-generation titanium sequencing platform. PloS One 6 (9).
Vignola, M., Werner, D., Wade, M.J., Meynet, P., Davenport, R.J., 2018. Medium shapes the microbial community of water filters with implications for effluent quality. Water Res. 129, 499–508.
Vries, D., Bertelkamp, C., Schoonenberg Kegel, F., Hofs, B., Dusseldorp, J., Bruins, J.H., de Vet, W., van den Akker, B., 2017. Iron and manganese removal: recent advances in modelling treatment efficiency by rapid sand filtration. Water Res. 109, 35–45.
Wakelin, S., Page, D., Dillon, P., Pavelic, P., Abell, G.C.J., Gregg, A.L., Brodie, E., DeSantis, T.Z., Goldfarb, K.C., Anderson, G., 2011. Microbial community structure of a slow sand filter schmutzdecke: a phylogenetic snapshot based on rRNA sequence analysis. Water Sci. Technol. Water Supply 11 (4), 426–436.
Wang, L., Wen, Y., Guo, X., Wang, G., Li, S., Jiang, J., 2010. Degradation of methamidophos by Hyphomicrobium species MAP-1 and the biochemical degradation pathway. Biodegradation 21 (4), 513–523.
Wang, K., Ye, X., Zhang, H., Chen, H., Zhang, D., Liu, L., 2016. Regional variations in the diversity and predicted metabolic potential of benthic prokaryotes in coastal northern Zhejiang, East China Sea. Sci. Rep. 6, 38709.
White 3rd, R.A., Power, I.M., Dipple, G.M., Southam, G., Suttle, C.A., 2015. Metagenomic analysis reveals that modern microbialites and polar microbial mats have similar taxonomic and functional potential. Front. Microbiol. 6, 966.
Wittebolle, L., Marzorati, M., Clement, L., Balloi, A., Daffonchio, D., Heylen, K., De Vos, P., Verstraete, W., Boon, N., 2009. Initial community evenness favours functionality under selective stress. Nature *458*, (7238), 623–626.
Zhang, S., Courtois, S., Gitungo, S., Raczko, R.F., Dyksen, J.E., Li, M., Axe, L., 2018. Microbial community analysis in biologically active filters exhibiting efficient removal of emerging contaminants and impact of operational conditions. Sci. Total Environ. 640–641, 1455–1464.
Zhang, W., Zhou, Y., Jeppesen, E., Wang, L., Tan, H., Zhang, J., 2019. Linking heterotrophic bacterioplankton community composition to the optical dynamics of dissolved organic matter in a large eutrophic Chinese lake. Sci. Total Environ. 679, 136–147.